

Floating Random Walk Based Capacitance Solver for VLSI Structures with Non-Stratified Dielectrics

Mingye Song*, Ming Yang†, Wenjian Yu‡

BNRist, Dept. Computer Science & Technology, Tsinghua University, Beijing 100084, China

Email: *songmy16@mails.tsinghua.edu.cn, †yang-m17@mails.tsinghua.edu.cn, ‡yu-wj@tsinghua.edu.cn

Abstract—In this paper, two techniques are proposed to enhance the floating random walk (FRW) based capacitance solver for handling non-stratified dielectrics in very large-scale integrated (VLSI) circuits. They follow an existing approach which employs approximate eight-octant transition cubes while simulating the structure with conformal dielectrics. Firstly, the symmetry property of the transition probabilities of the eight-octant cube is revealed and utilized to derive an on-the-fly sampling scheme during the FRW procedure. This avoids the pre-characterization, saves substantial memory, and improves computational accuracy for extracting the structure with non-stratified dielectrics. Then, the space management technique is extended to improve the runtime efficiency for simulating structures with thousands of non-stratified dielectrics. Numerical experiments are carried out to validate the proposed techniques and show their effectiveness for handling structures with conformal dielectrics and air bubbles. Moreover, the extended space management brings up to 1441X speedup for handling structures with from several thousand to nearly one million non-stratified dielectrics.

Index Terms—Capacitance extraction, non-stratified dielectric, floating random walk, space management.

I. INTRODUCTION

Due to the advantages on scalability and reliability, the floating random walk (FRW) algorithm has been widely adopted for the capacitance extraction of current very large-scale integrated (VLSI) circuits [1], [2]. Compared to the deterministic methods [3], [4], the FRW method is more stable in accuracy and more scalable to large structures, due to its nature of a discretization-free method. Recently, the FRW method has been extended to efficiently deal with cylindrical inter-tier-vias in 3-D ICs [5], the non-Manhattan conductors [6], and general-shape floating metals [7]. For the variation-aware capacitor modeling, an efficient technique based on the FRW method was also developed [8].

Under modern manufacturing technologies, conductors in VLSI circuits are separated by multiple stratified or conformal dielectrics. For better performance, air bubble as a special dielectric with the lowest permittivity may also be introduced [9]. However, the conformal dielectrics and air bubbles are not stratified dielectrics and they bring challenges to the capacitance field solver [4]. To handle conformal dielectric, an approach was proposed for the FRW method in [10], which utilizes a kind of eight-octant transition cube and equivalent permittivities. With the approach, a large amount of surface Green's function tables (GFTs) have to be pre-calculated prior to the capacitance extraction. So, it causes large cost of pre-

characterization and runtime memory usage (>1.6 GB), and induces error while matching the actual eight-octant transition cubes with the pre-characterized ones.

In this work, we improve the FRW based capacitance solver for extracting VLSI structures with non-stratified dielectrics. The major contributions are as follows.

- We reveal that the transition probabilities of the eight-octant transition cube have the symmetry property with scaling. Based on it, an on-the-fly sampling scheme in the FRW procedure is proposed, which avoids the pre-calculation and runtime memory cost for characterizing the eight-octant transition cubes. And, the improved FRW algorithm is more accurate than the approach in [10] as no interpolation computation is needed.
- In order to efficiently handle structures with a large quantity of non-stratified dielectrics, the space management technique in [11] for conductors is extended. By introducing a “dielectric” candidate list to each spatial cell and efficiently constructing the extended space management structure, we greatly reduce the runtime of FRW algorithm for handling structure with non-stratified dielectric, without loss of accuracy.
- Numerical experiments on structures with conformal dielectrics and air bubbles have been carried out. The results demonstrated the effectiveness and accuracy of the improved FRW solver through the comparison with an existing FRW solver [12] and Raphael [3]. They also showed that the extended space management technique brings tens to thousands times speedup to the FRW procedure for large VLSI structures.

II. BACKGROUND

A. The Floating Random Walk Method

The FRW method for capacitance extraction is derived from the integral formula for electric potential [13], [14]:

$$\phi(\mathbf{r}) = \oint_S P(\mathbf{r}, \mathbf{r}^{(1)})\phi(\mathbf{r}^{(1)})d\mathbf{r}^{(1)}, \quad (1)$$

where $\phi(\mathbf{r})$ is the potential of point \mathbf{r} and $P(\mathbf{r}, \mathbf{r}^{(1)})$ is called surface Green's function. The domain enclosing \mathbf{r} is called transition domain, whose surface is S . $P(\mathbf{r}, \mathbf{r}^{(1)})$ can be regarded as a probability density function. With Monte Carlo method, $\phi(\mathbf{r})$ can be estimated by the mean of $\phi(\mathbf{r}^{(1)})$ values.

When computing the capacitances related to a master conductor i , one should first construct a Gaussian surface G_i

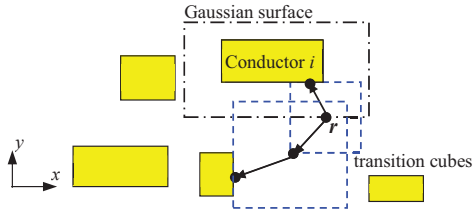


Fig. 1. Two random walks starting from r (denoted by consecutive segments with arrows) in the FRW method for capacitance simulation (2-D top view).

enclosing it (see Fig. 1). According to the Gauss theorem, the charge of conductor i is:

$$Q_i = \oint_{G_i} F(\mathbf{r}) g \oint_{S^{(1)}} \omega(\mathbf{r}, \mathbf{r}^{(1)}) \tilde{P}(\mathbf{r}, \mathbf{r}^{(1)}) \phi(\mathbf{r}^{(1)}) d\mathbf{r}^{(1)} d\mathbf{r}, \quad (2)$$

where $F(\mathbf{r})$ is the dielectric permittivity at point \mathbf{r} , $\tilde{P}(\mathbf{r}, \mathbf{r}^{(1)})$ is, probably different from $P(\mathbf{r}, \mathbf{r}^{(1)})$, for sampling on $S^{(1)}$, and $\omega(\mathbf{r}, \mathbf{r}^{(1)})$ is called weight value [13], [14]. Thus, Q_i can be estimated as the stochastic mean of sampled values on G_i , which is further the mean of sampled potentials on $S^{(1)}$ multiplying the weight value. If the potential of a sample point $\mathbf{r}^{(1)}$ is unknown, (1) is substituted into (2) recursively. The computation can be regarded as a floating random walk (FRW) procedure. The walk starts from the Gaussian surface, and repeatedly jumps until reaching conductor surface. After performing a number of walks, the stochastic mean of the weight values for the walks terminating at conductor j is capacitance C_{ij} between conductors i and j .

Each FRW includes a sequence of hops, each of which is from the center of a transition cube T to a random point selected following a certain surface Green's function. In practice, this random sampling is realized by first discretizing T 's surface into $6n^2$ panels and obtaining the transition probabilities to the panels, and then randomly choosing a panel [10], [14]. The surface Green's function for the transition onto T 's surface depends on dielectric configuration in T . Usually, the transition probabilities are pre-calculated and stored as the tables (called GFTs) for transition cubes with certain dielectric configurations [14]. By loading these tables before performing FRWs, one can make hops executed quickly.

B. The Existing Approach to Handle Conformal Dielectrics

Several approaches for precharacterizing the transition cubes with multilayer dielectrics have been proposed [10], [14], to deal with the stratified dielectrics in practical capacitance extraction. However, they are not applicable to structures with conformal dielectrics (or other non-stratified dielectrics), for which the transition cubes containing both horizontal and vertical variation of dielectrics are involved. It is impossible to use a finite number of dielectric configurations to cover all transition cubes encountered in the FRW based capacitance extraction for a structure with non-stratified dielectrics.

To tackle this problem, an approximate approach was proposed in [10] for handling conformal dielectric. It pre-characterizes a so-called eight-octant transition cube, of which each octant contains a homogeneous dielectric (as shown in Fig. 2(a)), with various configurations of dielectric permittivities. During the FRW procedure, the transition cube with both

horizontal and vertical dielectric variation (occurring around conformal dielectric, as shown in Fig. 2(b)) is approximated by the eight-octant transition cube with the permittivity of each octant obtained as the volume weighted average permittivity. Then, the transition probabilities of this transition cube are obtained from some pre-calculated GFTs for the eight-octant transition cubes and the linear interpolation calculation [15].

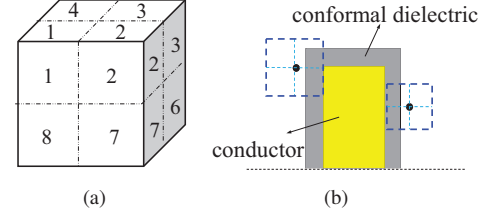


Fig. 2. (a) An eight-octant transition cube where each octant contains a homogenous dielectric (the octants are numbered). (b) The cross-section view of a conformal dielectric (in gray) and transition cubes (in blue) near it.

The approach using eight-octant transition cubes exhibits satisfied accuracy for extracting structures with conformal dielectrics, and is better than using a kind of “intrusive-type” transition cubes to approximate the transition cubes near conformal dielectrics [10]. However, pre-characterizing these eight-octant transition cubes still consumes a lot of computation and runtime memory usage. Notice that the GFT for an eight-octant cube with permittivities $\varepsilon_1, \varepsilon_2, \dots, \varepsilon_8$ is the same as that for an eight-octant cube with permittivities $\varepsilon_1/\varepsilon_{max}, \varepsilon_2/\varepsilon_{max}, \dots, \varepsilon_8/\varepsilon_{max}$, where $\varepsilon_{max} = \max\{\varepsilon_i\}$. So, the cube can be characterized by the normalized permittivities $\{\varepsilon_i/\varepsilon_{max}\}$. Although there are infinite values of these normalized permittivities, only considering some discrete normalized permittivities is often sufficient. Suppose for each octant its normalized permittivity ranges from 0.5 to 1 with discretized step s . The number of possible eight-octant configurations will be $(0.5/s+1)^8 - (0.5/s)^8$. Based on the Polya's enumeration theorem [16] and considering the symmetry, one can reduce the number of configurations to:

$$N_{GFT} = \frac{1}{24} \left[\left(\frac{1}{2s} + 1 \right)^8 + 6 \left(\frac{1}{2s} + 1 \right)^2 + 17 \left(\frac{1}{2s} + 1 \right)^4 - \frac{1}{(2s)^8} - \frac{3}{(2s)^2} - \frac{17}{(16s^4)} \right]. \quad (3)$$

Suppose $s = 0.1$, which means we only let the normalized permittivity be 0.5, 0.6, 0.7, 0.8, 0.9, or 1, and each GFT needs about 30 KB storage [10]. Then, the memory cost for these eight-octant cubes' GFTs will be 1.6 GB. If using smaller value of s to pursue higher accuracy, this memory cost will become even larger.

In this work, an on-the-fly approach sampling the eight-octant transition cubes is proposed. It avoids the pre-characterization and thus largely saves memory. It doesn't need linear interpolation, resulting in the FRW method with higher accuracy than [10] for handling non-stratified dielectrics.

III. AN IMPROVED FRW METHOD WITH ON-THE-FLY SAMPLING ON THE EIGHT-OCTANT TRANSITION CUBES

In this section, we reveal the special properties of the transition probabilities associated with the eight-octant trans-

sition cube, and then derive the improved FRW algorithm for handling non-stratified dielectrics.

A. The Symmetry Property of Transition Probabilities

The dielectric configuration of an eight-octant transition cube T can be described by the eight dielectric permittivities: $\varepsilon_1, \varepsilon_2, \dots, \varepsilon_8$. With the finite difference method (FDM), we can numerically compute the transition probabilities $\{p_i\}$ [14], following which a random hop is conducted from T 's center C to its surface. The key point is to obtain the relationship between the potential of point C and the potential of T 's surface points. The FDM grids and relevant concepts are illustrated in Fig. 3.

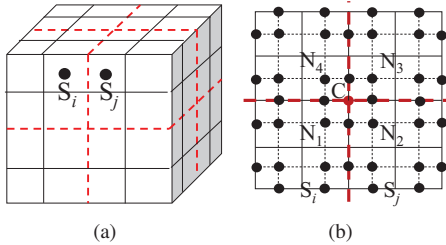


Fig. 3. The FDM grids for an eight-octant transition cube, where red dashed lines outline the octants. (a) The cube is evenly divided into $n \times n \times n$ cells. S_i and S_j are two examples of surface panel's center. (b) The top view of the eight-octant cube with the FDM grids imposed. Black points are grid points. C is the cube's center, and $N_1 \sim N_4$ are its four neighbor grid points (the other four neighbor grid points coincide with them in this view).

With exhaustive experiments and theory analysis, we find out that the transition probabilities associated with the eight-octant transition cube have the following symmetry property.

Proposition 1: For two panel center points S_i and S_j in different octants of an eight-octant transition cube T , if they have symmetric positions with respect to T 's center C , the transition probabilities to them, namely p_i and p_j , satisfy:

$$\frac{p_i}{\varepsilon_i} = \frac{p_j}{\varepsilon_j} = \frac{8\bar{p}_i}{\sum_{i=1}^8 \varepsilon_i}, \quad (4)$$

where ε_i and ε_j are the permittivities of the octants containing S_i and S_j , respectively. $\varepsilon_1 \sim \varepsilon_8$ are all the permittivities describing T , and \bar{p}_i denotes the transition probability from C to S_i in a single-dielectric transition cube with the same size and FDM discretization as T .

The proof of Proposition 1 can be accomplished based on the theory of random walk and stochastic process. Due to page limit, we omit it here. Instead, we show some experimental results to validate the symmetry property. Consider two eight-octant transition cubes with the following permittivities:

Eight-octant cube 1: $\varepsilon_i = 1, 1 \leq i \leq 4; \varepsilon_j = 0.5, 5 \leq j \leq 8$;

Eight-octant cube 2: $\varepsilon_1 = 1, \varepsilon_2 = 0.9, \varepsilon_3 = 0.8, \varepsilon_4 = 0.7, \varepsilon_5 = 1, \varepsilon_6 = 0.9, \varepsilon_7 = 0.6, \varepsilon_8 = 0.7$.

We have developed a program similar to TechGFT in [14] to generate the transition probabilities for the both eight-octant cubes. The number of segments along cube edge is $n = 32$. With these probabilities we draw the scatter plots. In Fig. 4(a), the transition probabilities to octant No. 1 and No. 8 in eight-octant cube 1 are shown. They are denoted by arrays $\mathbf{p1}$ and $\mathbf{p8}$, respectively. We sort array $\mathbf{p1}$ in ascending order and then

rearrange the elements in $\mathbf{p8}$ so that $\mathbf{p1}[i]$ and $\mathbf{p8}[i]$ correspond to two panels which have same positions with respect to the cube's center. Then, we take the elements in $\mathbf{p1}$ and $\mathbf{p8}$ as

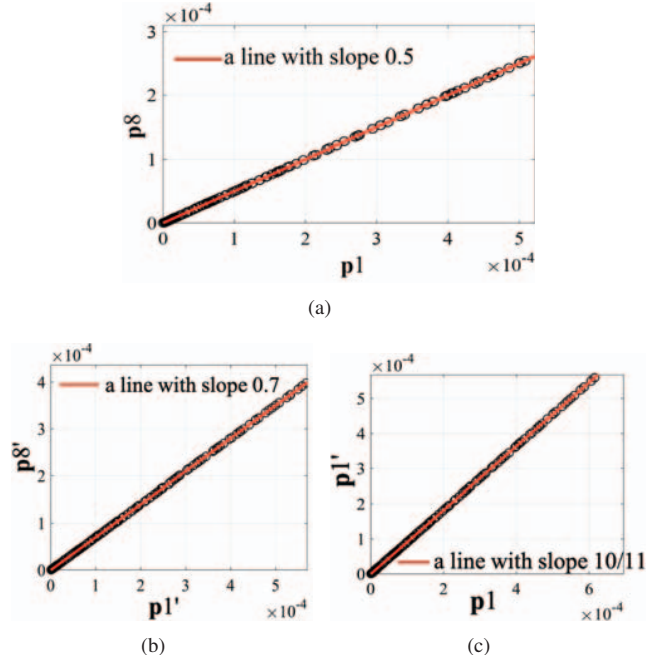


Fig. 4. The ratio of the transition probabilities to two different octants is a constant if they correspond to two panels having same position with respect to the center of eight-octant transition cube. (a) The two octants are No. 1 and 8 in the eight-octant cube 1, with permittivities 1 and 0.5 respectively. (b) The two octants are No. 1 and 8 in the eight-octant cube 2, with permittivities 1 and 0.7 respectively. (c) The two octants are the No. 1 octants in the two eight-octant cubes respectively. The permittivities of the eight-octant cubes are $(1, 1, 1, 1, 0.5, 0.5, 0.5, 0.5)$ and $(1, 0.9, 0.8, 0.7, 1, 0.9, 0.6, 0.7)$ respectively. x -coordinates and y -coordinates to draw the data points. We see that the data are on a line with slope 0.5, which means each probability to octant No. 8 is 0.5 times its correspondence to octant No. 1. This is because $\varepsilon_8 = 0.5\varepsilon_1$ in the eight-octant cube 1, and it validates the first equality in (4). Similar results are shown in Fig. 4(b), where the transition probabilities to octant No. 1 and No. 8 in eight-octant cube 2 are plotted. Because $\varepsilon'_8 = 0.7\varepsilon'_1$ in the eight-octant cube 2, the data are on the straight line with slope 0.7. We have also looked at other octant pairs in these two eight-octant cubes. The data of their transition probabilities all validate the first equality in the conclusion of Proposition 1.

To validate the second part of (4), we compare the transition probabilities to the No. 1 octants in eight-octant cube 1 and 2, which are denoted as arrays $\mathbf{p1}$ and $\mathbf{p1}'$, respectively. $\mathbf{p1}[i]$ and $\mathbf{p1}'[i]$ correspond to same panel in octant No. 1, and we use them as x -coordinate and y -coordinate respectively to draw the data points in Fig. 4(c). From the figure we see that the data are on a straight line with slope 10/11. This validates the latter equality in (4) which states that the transition probability equals to a constant multiplied by the ratio of the current octant's permittivity to the sum of eight permittivities. It is verified as regards

$$\frac{\mathbf{p1}'[i]}{\mathbf{p1}[i]} = \frac{1/(1+0.9+0.8+0.7+1+0.9+0.6+0.7)}{1/(1+1+1+1+0.5+0.5+0.5+0.5)} = \frac{6}{6.6} = \frac{10}{11}. \quad (5)$$

We have similarly inspected the probabilities to other octants in the two eight-octant cubes, and found out similar proportion relationships, which validates the second equality as well.

B. Improved FRW Algorithm with On-the-Fly Sampling

Proposition 1 implies the following statements for an eight-octant transition cube T,

(1) The sum of transition probabilities from T's center to the surface of an octant is proportional to the octant's dielectric permittivity;

(2) For a given octant of T, the transition probabilities to its surface are constant multiplies of those for a single-dielectric transition cube.

So, we can obtain the GFT for any eight-octant transition cube from the GFT for a single-dielectric transition cube with same discretization. The single-dielectric GFT can be pre-calculated analytically [13] and is always needed. So, this enables the on-the-fly generation of the accurate GFT for an eight-octant transition cube. In practice, we first randomly choose an octant following the probabilities proportional to the eight octants' permittivities. Then, for selecting a point on the chosen octant's surface we just follow the single-dielectric GFT. This approach induces no precharacterization computation or memory cost.

With the on-the-fly sampling on the eight-octant cubes, the FRW algorithm for simulating structure with non-stratified dielectrics is proposed as Algorithm 1.

IV. AN EXTENDED SPACE MANAGEMENT TECHNIQUE

A. Motivation and Background

An important step in Alg. 1, see Step 10 and 11, is to calculate the volume weighted average permittivity. Obviously, it is time-consuming to figure out whether the transition cube intersects any non-stratified dielectrics by means of traversing all these dielectrics. When thousands of hops are performed and hundreds of dielectrics are involved, the brute force method based on traversing the dielectrics will induce excessive computation. In order to calculate the volume of each dielectric in the transition cube as fast as possible, a space management structure is required.

In Step 9 of Alg. 1, the largest conductor-free transition cube is commonly used in order to terminate a walk earlier. This asks for finding the nearest conductor. To be efficient, a space management approach of conductors was presented in [11] for calculating the distance from the current point to the nearest conductor as fast as possible during the random walk.

The key technique is to build a space management structure to record the conductors' information in prior to the FRW procedure. Usually, the problem domain is divided into small subdomains called spatial cells, and each cell is attached with a candidate list of conductors such that for any point in the cell its nearest conductor is in the list. A neighbor region is also defined through inflating the cell with the extension size d_{nb} (see Fig. 5). In order to speed up the construction of space management structure, only the conductors in a cell's neighbor region are checked. To make sure that it is conductor-free, the

Algorithm 1 The FRW for handling non-stratified dielectrics

```

1: Load the pre-calculated transition probabilities (GFTs) and
   weight values (WVTs) for the unit-size single-dielectric
   and multilayer-dielectric cubes;
2: Construct a Gaussian surface for master conductor  $i$ ;
3:  $C_{ij} := 0, \forall j; npath := 0$ ;
4: repeat
5:    $npath := npath + 1$ ;
6:   Randomly pick a point on the Gaussian surface, and
      construct a cubic transition domain  $T$  (may contain
      multilayer dielectrics) taking the point as center;
7:   Randomly pick a point on  $T$ 's surface according to the
      transition probabilities inferred from the loaded GFTs,
      and then obtain the weight value  $\omega$  with WVTs;
8:   while the current point is not on a conductor do
9:     Make the largest conductor-free transition cube  $T$ ;
10:    if  $T$  intersects any non-stratified dielectric then
11:      Approximate  $T$  with an eight-octant transition
          cube  $\tilde{T}$  by calculating volume weighted average
          permittivity;
12:      Randomly pick a point on the surface of  $\tilde{T}$  using
          the proposed on-the-fly sampling approach;
13:    else
14:      Randomly pick a point on  $T$ 's surface, according to
          the single-dielectric or multilayer-dielectric GFTs;
15:    end if
16:   end while
17:    $C_{ij} := C_{ij} + \omega; //$  the current point is on conductor  $j$ .
18: until the termination criterion is satisfied
19:  $C_{ij} := C_{ij}/npath, \forall j$ .

```

transition cube is established with the smaller length between the minimum distance to candidate conductors and that to the boundary of neighbor region (such as d_b rather than d_2 in Fig. 5). Thus, it is guaranteed that any transition cube does not intersect any conductor and has sufficiently large size [11].

B. Space Management Structure for Non-Stratified Dielectrics

It can be inferred from the above paragraph that the transition cube constructed from the point inside the cell cannot exceed the range of the neighbor region. Therefore, we can store the non-stratified dielectrics inside the spatial cell's neighbor region as another candidate list for further use in the random walk. Instead of all the non-stratified dielectrics, only traversing this candidate list helps to find out whether the transition cube intersects any non-stratified dielectrics. Thus, a space management technique for non-stratified dielectrics can

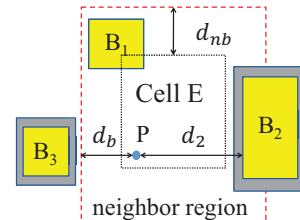


Fig. 5. The illustration of a spatial cell E and its neighbor region, with conductor blocks marked in yellow and non-stratified dielectrics in gray.

be developed. In [11], experimental results show that among several space management structures the grid-Octree hybrid approach achieves the best performance. Therefore, we extend it to handle non-stratified dielectrics. Algorithm 2 describes the construction of the grid-Octree hybrid structure.

Algorithm 2 Generate the Extended Space Management Structure for Handling Non-Stratified Dielectrics

```

1: Divide the problem domain into  $n_x \times n_y \times n_z$  grid cells;
2: Set a proper  $d_{nb}$ ;
3: for each grid cell  $E_i$  do
4:   Define an Octree root node  $R_i$  for the domain of  $E_i$ ;
5:   for each non-stratified dielectric  $D$  do
6:     if  $D$  intersects the neighbor region of  $R_i$  then
7:       Add  $D$  to  $R_i$ 's "dielectric" candidate list;
8:     end if
9:   end for
10:  for each conductor  $B$  do
11:    InsertToOctree( $B, R_i$ );
12:  end for
13: end for
```

In Alg. 2, a grid-based structure is first used to represent the problem domain, where each grid cell is a cube. Then, an Octree root node is defined for each cell, which is attached by two initial candidate lists for conductor and for non-stratified dielectric. Finally, the Octree nodes grow up, while nearby conductors and non-stratified dielectrics are inserted into the candidate lists successively. Step 11 in Alg. 2 contains three steps to construct an Octree structure. Firstly, conductors are checked through judging the domination relationship [11]. Subsequently, in condition that the length of "conductor" candidate list is larger than the prespecified threshold, Octree node will be split into 8 child nodes. After splitting, the dielectrics in the candidate list of the parent node will be inserted into the child nodes if they intersect the child nodes' neighbor region, and this function is called recursively to insert conductor into each child node.

Another strategy for the construction is to form a "dielectric" candidate list for each leaf node after constructing the original space management structure for conductors. The critical step is to check whether the non-stratified dielectric intersects the node's neighbor region. The average number for calculating the spatial relationship on each non-stratified dielectric with this strategy is the number of the leaf nodes in the Octree. In contrast, the average number for the same calculation in Alg. 2 is proportional to the height of the Octree. It is obvious that the number of leaf nodes increases faster than the height in Octree structure when the Octree structure grows up. So, Alg. 2 achieves better performance in the construction of the space management.

In Step 10 of Alg. 1, we can check whether a transition cube intersects any non-stratified dielectrics based on the "dielectric" candidate list, rather than traversing all the non-stratified dielectrics. This makes the checking time largely reduced because the average length of the "dielectric" candidate list is much smaller than that of all the non-stratified dielectrics,

which will be demonstrated in our experiments.

V. EXPERIMENTAL RESULTS

We have implemented the 3-D FRW algorithm for capacitance extraction, and the techniques proposed in this work. It is used to simulate several VLSI structures with conformal dielectrics and air bubbles. The results are compared with Raphael [3] and RWCap3 [12]. All experiments are carried out on a Linux server with Intel Xeon E5-2650 2.0 GHz CPU.

Case 1~2 are based on Case 1 (180-nm technology) and Case 4 (45-nm technology) in [14] by adding a conformal dielectric around the three wires in M2 layer (see Fig. 6).

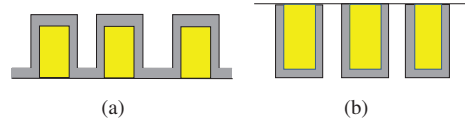


Fig. 6. A portion of cross-section view of Case 1 and 2. The coating conformal dielectric has the same permittivity as its adjacent dielectric. (a) Case 1, based on Case 1 in [14]. The thickness of conformal dielectric is 40nm. (b) Case 2, based on Case 4 in [14]. The thickness of conformal dielectric is 5nm.

Case 3~6 include 3 parallel wires in M2 layer and 10 crossing parallel wires in M3 layer. The M2 wires are coated by different conformal dielectrics and embedded in stratified dielectrics. The size of each wire is 45nm×400nm×90nm. The spacing between wires is 45nm for Case 3~5 and 28nm for Case 6. For Case 5, there are multiple conformal dielectrics.

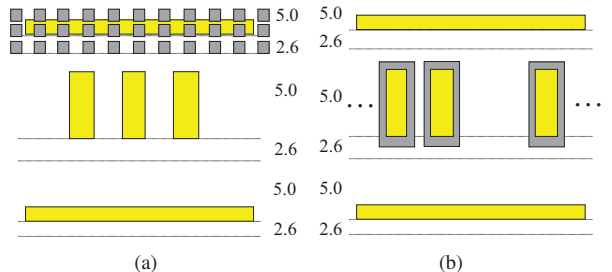


Fig. 7. (a) The cross-section view of Case 8. The gray cubes are air bubbles, whose permittivity is 1. (b) A part of the cross-section view of Case 9. The permittivity of the conformal dielectric is 3.7. The relative permittivity of each stratified dielectric is labeled.

Case 7~8 are three-parallel-wire structures between two parallel conductor plates, constructed based on Fig. 9 in [9]. The size of wire is 45nm×450nm×90nm with 45nm spacing. Above the wires there are a 11×157×2 array of air cubic bubbles in Case 7 and 11×209×3 bubbles in Case 8 (see Fig. 7(a)), whose size is 13.4nm and spacing is 16.7nm. The aim of the bubbled layer is to reduce parasitic capacitance.

Case 9 is a very large case containing 2302984 conductors in 3 mental layers, and each of 774911 conductors in M2 layer is enclosed with one conformal dielectric (see Fig. 7(b)).

For Case 1~6, one of the M2 wires is set as the master conductor and its capacitances are extracted. The termination criterion for all FRW algorithms on these cases is 0.5% 1- σ error on the total capacitance. For Case 1 and 2, the results of RWCap3 and the proposed Algorithm 1 are listed in Table I. #walk means the number of FRW paths, while #hop means the average number of hops per walk. In the two cases,

the conformal dielectric has same permittivity as its adjacent dielectric. So, if we remove the interface between them we can extract the cases with RWCap3. We see that the results validate our algorithm's accuracy for handling non-stratified dielectric. As extra geometric operations are needed to process non-stratified dielectric, our algorithm runs a little slower than RWCap3. As for the memory usage, the proposed one does not cost extra memory. They both cost 50.5 MB memory.

TABLE I
THE COMPUTATIONAL RESULTS FOR THE FIRST TWO CASES

Case	Algorithm	#walk	#hop	Time(s)	Cap.(fF)	Error(%)
Case 1	RWCap3	133K	65.9	2.91	1.870	-
	Our Alg.	132K	64.9	5.63	1.849	-1.1
Case 2	RWCap3	50K	70.7	1.13	0.364	-
	Our Alg.	62K	57.3	2.29	0.362	-0.5

Then, we set the permittivity of the conformal dielectrics in Case 1 and 2 to 7.0 and obtain two actual conformal cases Case 1' and Case 2'. Along with Case 3~6 they are all simulated with the proposed algorithm and the golden-standard tool Raphael [3]. The results are listed in Table II. From the table we see the good accuracy of the proposed method. With the on-the-fly sampling on eight-octant transition cubes, the improved FRW algorithm ensures good accuracy. As for the memory usage, all cost 50.5 MB.

TABLE II
THE COMPUTATIONAL RESULTS FOR THE FIRST SIX CASES WITH NON-STRATIFIED DIELECTRICS

Case	#walk	#hop	Time(s)	Cap.(fF)		Error (%)
				Our Alg.	Raphael	
Case 1'	103K	52.5	3.74	2.060	2.050	0.5
Case 2'	48K	52.9	1.24	0.401	0.399	0.5
Case 3	67K	68.9	2.09	0.104	0.105	-1.0
Case 4	72K	82.4	2.73	0.106	0.105	0.9
Case 5	65K	67.4	2.14	0.104	0.105	-1.0
Case 6	34K	38.6	0.56	0.161	0.159	1.2

We use Case 7~9 to evaluate the proposed space management approach in Section IV. The results are listed in Table III. T_{sp} denotes the time for the construction of the space management, and T_{frw} denotes the time for the FRW procedure executed on 16 threads. The termination criterion is 1% 1- σ error. For the largest case, namely Case 9, the result reveals that our algorithm can be 1441X faster than the brute force method traversing all non-stratified dielectrics (3.8s vs. 5478s). Although T_{sp} increases, the overall runtime still achieves 47X (118s vs. 5508s) speedup. This validates the efficiency of extended space management for large structures. Case 7 is also calculated with Raphael. The result on total capacitance is 89.53 aF. Regarding it as the standard, we see that the error of our method is only -1.2% (88.44 vs 89.53). This again validates the accuracy of proposed technique. For Case 8 and 9, the result of Raphael is not available.

VI. CONCLUSIONS

The existing FRW based capacitance solvers employ a lot of offline computation to pre-calculate the transition probabilities for transition cubes approximating all possible transition cubes occurring around conformal dielectric. We improve them based

TABLE III
THE COMPARISON BETWEEN THE BRUTE FORCE APPROACH AND THE PROPOSED TECHNIQUE FOR SPACE MANAGEMENT

Case	Algorithm	Memory(MB)	Cap.(aF)	T_{sp} (s)	T_{frw} (s)
Case 7	brute force	52.7	88.44	0.02	89.96
	proposed	52.7	88.44	0.02	4.94
Case 8	brute force	54.5	89.05	0.03	176.3
	proposed	54.5	89.05	0.03	8.26
Case 9	brute force	1140	761.6	29.9	5478
	proposed	1200	761.6	114	3.78

on the symmetry property of the transition probabilities of the eight-octant cube and derive an on-the-fly sampling scheme. Besides, the space management technique is extended to improve the runtime performance during the FRW procedure. Experiments validate the accuracy and efficiency of our proposed algorithm even with considerably large structures.

VII. ACKNOWLEDGEMENT

M. Song and M. Yang contributed equally to this work, which is supported by Beijing National Research Center for Information Science and Technology (BNR2019ZS01001).

REFERENCES

- [1] W. Yu and X. Wang, *Advanced Field-Solver Techniques for RC Extraction of Integrated Circuits*, Springer Inc., Apr. 2014.
- [2] T. Dillinger, “Field-solver parasitic extraction goes mainstream,” 2017, <https://www.semiwiki.com/forum/content/7154-field-solver-parasitic-extraction-goes-mainstream.html>.
- [3] Synopsys Inc., “Raphael,” <https://www.synopsys.com/silicon/tcad/interconnect-simulation/raphael.html>.
- [4] Y. Zhou, Z. Li, and W. Shi, “Fast capacitance extraction in multilayer, conformal and embedded dielectric using hybrid boundary element method,” in *Proc. DAC*, 2007, 835840.
- [5] C. Zhang, W. Yu, Q. Wang, et al., “Fast random walk based capacitance extraction for the 3-D IC structures with cylindrical inter-tier-vias,” *IEEE Trans. CAD*, 34(12): 1977-1990, 2015.
- [6] Z. Xu, C. Zhang, and W. Yu, “Floating random walk based capacitance extraction for general non-Manhattan conductor structures,” *IEEE Trans. CAD*, 36(1): 120-133, 2017.
- [7] W. Yu, Z. Xu, B. Li, et al., “Floating random walk based capacitance simulation considering general floating metals,” *IEEE Trans. CAD*, 37(8): 1711-1715, 2018.
- [8] P. Maffezzoni, Z. Zhang, S. Levantino, et al., “Variation-aware modeling of integrated capacitors based on floating random walk extraction,” *IEEE Trans. CAD*, 37(10): 2180-2184, 2018.
- [9] G. Kansal, A. Sharma, I. Raza, 2014, “Decreasing parasitic capacitance in IC layouts,” <https://www.edn.com/design/analog/4426479/Decreasing-parasitic-capacitance-in-IC-layouts>.
- [10] G. Rollins, (Jul. 2010). “SESS Rapid3D 20X Performance Improvement,” [Online]. (Power Point slideshow, 36 pages).
- [11] C. Zhang and W. Yu, “Efficient space management techniques for large-scale interconnect capacitance extraction with floating random walks,” *IEEE Trans. CAD*, 32(10): 1633-1637, 2013.
- [12] “RWCAP,” http://numbda.cs.tsinghua.edu.cn/download/RWCAP_v3.html.
- [13] Y. Le Coz and R. B. Iverson, “A stochastic algorithm for high speed capacitance extraction in integrated circuits,” *Solid-State Electronics*, 35(7): 1005-1012, 1992.
- [14] W. Yu, H. Zhuang, C. Zhang, et al., “RWCAP: A floating random walk solver for 3-D capacitance extraction of VLSI interconnects,” *IEEE Trans. CAD*, 32(3): 353-366, 2013.
- [15] Z. Xu, W. Yu, C. Zhang, et al., “A parallel random walk solver for the capacitance calculation problem in touchscreen design,” in *Proc. GLSVLSI*, May 2016, 1661-1666.
- [16] Sasha Patotski, “Polya Enumeration Theorem,” 2015, <http://pi.math.cornell.edu/~apatotski/IHS2015/Lecture10.pdf>.